ACS OMEGA

http://pubs.acs.org/journal/acsodf

Article

Template-Less and Surfactant-Less Synthesis of CeO_2 Nanostructures for Catalytic Application in *Ipso*-hydroxylation of Aryl Boronic Acids and the aza-Michael Reaction

Tulan Chandra Saikia, Xavy Borgohain, Saddam Iraqui, and Md. Harunar Rashid*

Cite This: *ACS Omega* 2022, 7, 42126–42137

Read Online

ACCESS | Metrics & More | Article Recommendations | Supporting Information

ABSTRACT: Due to its excellent physicochemical properties, CeO_2 has found great importance as an electrochemical and in electronics, photocatalysis, sensing, and heterogeneous catalysis. Herein, we report the surfactant-less and template-less synthesis of CeO_2 nanostructures by the hydrothermal method. The synthesized CeO_2 nanostructures have been characterized in detail by electron microscopy, spectroscopy, diffractometry, and other analytical methods. The XRD studies revealed the formation of pure crystalline CeO_2, possessing a cubic fluorite structure with an average crystallite size of 15.6 to 16.4 nm. Electron microscopy studies reveal the formation of cube-shaped CeO_2 nanostructures with sizes below 25 nm. The cube-shaped CeO_2 nanostructures exhibited a higher BET surface area compared to their bulk counterparts. The XPS analysis has confirmed the existence of Ce in the mixed oxidation states of +3 and +4, while O is present as O^{2-} in the sample. The as-synthesized CeO_2 nanostructures exhibit excellent catalytic activity in both the *ipso*-hydroxylation of aryl boronic acids and the aza-Michael reaction. The analysis of the used catalyst has confirmed its stability under the reported reaction conditions. The catalysts retain their catalytic activity up to the fifth run in both types of reactions, which is economically beneficial for industrial application.

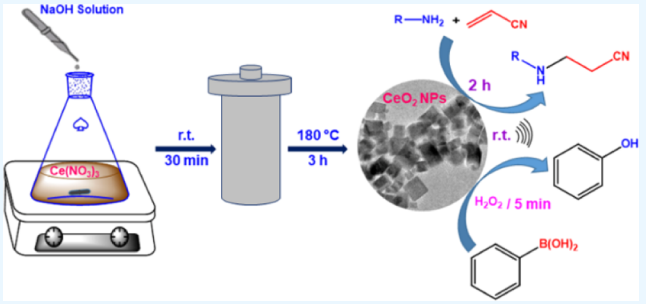

1. INTRODUCTION

Cerium is the second element in the lanthanide family and the most abundant rare earth metal.[1] In the ground state, one electron of cerium enters the 4f orbital, which has nearly the same energy as that of the outer 5d and 6s orbitals (Ce = [Xe] $4f^1$ $5d^1$ $6s^2$). For this reason, cerium shows exceptional cycling or redox properties between its two ionic states, Ce^{3+} and Ce^{4+}.[2,3] Cerium is the only element which shows a solid-state critical point.[1] Although cerium forms two oxides, viz., cerium(IV) oxide (CeO_2) and cerium(III) oxide (Ce_2O_3), cerium(IV) oxide, commonly known as ceria, is more stable compared to Ce_2O_3.[4] Due to the reduced size, CeO_2 nanostructures possess remarkable properties compared to their bulk counterparts.[5] Among the three low index planes, viz., (100), (110), and (111) of cubic fluorite structure of CeO_2, the (111) plane is the most stable one, while the planes (100) and (110) are more reactive because of the ease with which lattice oxygen migrates in these planes.[5] The existence of Ce^{4+}/Ce^{3+} redox couples and high mobility of oxygen vacancies make CeO_2 NPs a suitable candidate for use as oxygen storage media, catalysts, adsorbents, sensors, and so forth.[6−13] Furthermore, the oxygen buffering capacity of CeO_2 makes it a potent catalyst for the oxidation of CO and other exhaust gases.[14] The crystal surfaces and plane properties of CeO_2 crystals determine the interaction of adsorbed molecules on the surface of CeO_2 NPs.[15] The literature reports revealed that CeO_2 exhibits a greater lattice expansion as the particle size decreases, leading to a decrease in its oxygen release and reabsorption capabilities.[15] The high unsaturation of CeO_2 contributes to the instability, which is accompanied by the restructuring of the surface and eventually affects the chemical reactivity of CeO_2 nanostructures.[15] Moreover, different active facets of CeO_2 NPs can be exposed by tuning the shapes and surface properties via different synthesis methods, thereby enhancing the chemical reactivity.[5]

In developing new synthetic methodologies, "green chemistry" has been a central issue for centuries, where the synthetic procedures without the green approach become incompetent with time.[16] Therefore, in designing a new synthetic methodology, it is desirable to use safe and cost-effective catalysts, reagents, and solvents, which can furnish high atom economy and minimize waste products.[17−19] Accordingly, the development of environmentally friendly and cost-effective catalytic

Received: July 21, 2022
Accepted: November 1, 2022
Published: November 11, 2022

systems for organic synthesis has been growing rapidly in recent years.[20,21] In the field of modern organic synthesis, phenols and their derivatives are considered to be important building blocks for various important compounds involving pharmaceutical, agrochemical, and natural products.[22−24] As a result, there have been several techniques for synthesizing phenols over the years, and traditionally, phenols were synthesized by pyrolysis of haloarenes[25] and the sodium salt of aryl sulfonic acids,[26] oxidation of cumene,[27] hydrolyses of aryl diazonium salts,[28] and so forth. However, most of the traditional synthesis procedures have less substrate scope in terms of yield and require very harsh conditions, such as the requirement of strong bases, high temperature and pressure, and so forth.[29] To overcome those demerits, the *ipso*-hydroxylation of aryl boronic acids has been adopted in recent times to synthesize phenols due to its various advantages such as the ease of conversion of aryl boronic acids into phenols, nontoxicity, and stability of aryl boronic acids against moisture.[30,31] Accordingly, different catalyst systems such as poly(*N*-vinylpyrrolidone)-H_2O_2 and poly(4-vinyl pyridine)-H_2O_2 complexes,[32] *N*-oxide,[33] hypervalent iodine (III),[34] supported Ag nanoparticles (NPs),[35,36] graphene oxide,[37] Cu_2O NPs,[38] ZnO NPs,[39,40] and Fe_2O_3/Al_2O_3 nanocomposites[41] have been reported recently by several research groups across the world for the oxidative hydroxylation of aryl boronic acid. In most of the reported protocols involving H_2O_2 as the oxidant, it has been observed that while trying to make a green catalytic system, they often underestimate the "atom economy" principle of green chemistry. For example, many reports are available in recent years where more than 1.5 equivalents of H_2O_2 was used as an oxidizing agent while carrying out the *ipso*-hydroxylation of aryl boronic acid.[30,37,42,43] Moreover, reports are also available on the *ipso*-hydroxylation of aryl boronic acids without the use of any oxidizing agent.[38,44] However, those protocols require prolonged reaction times and high temperatures, yet the yield of the product is low, which is another disadvantage for commercial use.[38,44] Herein, we report the development of a catalyst system for *ipso*-hydroxylation of boronic acids associated with a high atom economy using CeO_2 nanostructures as reusable catalysts.

The C−N bond forming reaction via the aza-Michael reaction is another vital reaction in synthetic organic chemistry for the synthesis of various bioactive molecules, β-amino nitriles, β-amino carboxylic acid derivatives, β-amino carbonyl derivatives, pharmaceutical ingredients, and so forth.[45−48] Aliphatic amines or cyclic amines usually undergo an aza-Michael reaction with acrylonitrile easily but aromatic amines not only take a longer time to undergo such reactions with acrylonitrile but also produce a poor yield of the product.[49,50] Traditionally aza-Michael addition reactions are carried out under very harsh conditions requiring strong acids or bases, high temperatures, and prolonged reaction times.[46,49,51,52] Further, the use of expensive solvents in those procedures limits their applicability in commercial application. To overcome those drawbacks, catalytic systems have been developed in recent years, which mostly involve nanomaterials,[53] ionic liquids,[54,55] metal−organic frameworks,[56,57] and so forth. However, the requirements of strong bases,[58] acid catalysts,[59] high reaction temperatures,[60] long reaction times,[61] and low yields of the product[46] are major drawbacks of those reported methods. More importantly, the developed catalytic systems for the aza-Michael reaction do not work at all for aromatic amines.[59] Herein, we also report the use of CeO_2 nanostructures as efficient and reusable heterogeneous catalysts for both the *ipso*-hydroxylation of boronic acids and the aza-Michael reaction in a moderately greener approach under ultrasonic vibration at room temperature.

2. EXPERIMENTAL SECTION

2.1. Reagents. Cerium nitrate hexahydrate [$Ce(NO_3)_3 \cdot 6H_2O$], sodium hydroxide (NaOH) pellet, and hydrogen peroxide (H_2O_2; 30% (w/w); aqueous) were purchased from Merck, India, and were used without further purification. Commercial CeO_2 powder (AR, 99.9%) was purchased from SRL, India. Aryl boronic acids, acrylonitrile, and the other amine substrates were purchased from Sigma-Aldrich and were used as received. The preparation of CeO_2 nanostructures was performed using double distilled water.

2.2. Synthesis of CeO_2 Nanostructures. To synthesize CeO_2 nanostructures, a hydrothermal method was adopted in the absence of any external capping agents. Typically, in a 100 mL stopper conical flask, 30 mL of $Ce(NO_3)_3 \cdot 6H_2O$ (0.8684 g) solution and 10 mL of NaOH (2.0 M) solution were taken and mixed for 10 min under magnetic stirring at room temperature. The resultant solution was then transferred into a 50 mL capacity autoclave, which was then placed in an oven preheated to 180 °C for ageing the reaction mixture for 3.0 h. The resulting product was then isolated by centrifugation at 9000 rpm for 10 min followed by dispersion of the product in water under ultrasonic vibration and centrifugation to get rid of the unreacted components. The process of redispersion and centrifugation was carried out three times followed by drying the wet product in a vacuum oven overnight at 60 °C. The dried product was labeled CeO-1. Another sample (CeO-2) was also prepared by the same method with the same concentration of the precursor salt, but the concentration of NaOH was doubled, that is, the final concentration is 1.0 M against 0.5 M in CeO-1. The as-synthesized products were analyzed using different modern instrumental techniques for characterization. The details of the instrumental techniques used for characterization are provided in the Supporting Information.

2.3. *Ipso*-hydroxylation of Aryl Boronic Acids. In a round bottom flask of capacity 25 mL, freshly prepared CeO_2 nanostructures (7.0 mg) and phenylboronic acid (1.0 mmol) were mixed under ultrasonic vibration (Aczet CUB 2.5; 40 kHz) using 3.0 mL of double distilled water as the solvent. After 2.0 min, 0.125 mL of H_2O_2 (30%; w/w) solution was poured into the reaction mixture under ultrasonic vibration. Thin-layer chromatography (TLC) was used to track the progress of the reaction. At the end of the reaction, the crude product present in the reaction mixture was dissolved in 50 mL of ethyl acetate taken in a 250 mL separating funnel. The organic layer was washed three times using a brine solution. The isolated organic layer was then filtered through anhydrous sodium sulfate to remove the residual water molecules, if any, present in the organic layer. The organic layer was then concentrated by removing ethyl acetate in a rotary evaporator at 40 °C. In the isolated concentrated solution of the product and ethyl acetate, an excess amount of *n*-hexane was added and shaken by hand for a minute. The resulting solution got split into two separate layers, and the upper layer was discarded. The pure products isolated from the bottom layer by removing *n*-hexane under vacuum were used for characterization by ^1H NMR and ^{13}C NMR spectroscopy.

https://doi.org/10.1021/acsomega.2c04614
ACS Omega 2022, 7, 42126−42137

2.4. aza-Michael Reaction Between Amines and Acrylonitrile. In a 25 mL round bottom flask water (3.0 mL), CeO_2 nanostructures (10.0 mg), K_2CO_3 (69.0 mg), and acrylonitrile (2.5 mmol) were mixed under ultrasonic vibration (Aczet CUB 2.5; 40 kHz). Additionally, in a separate 10 mL vial, 1.0 mmol aniline was mixed with 0.5 mL of ethanol, and the whole content was poured into the round bottom flask containing the reaction mixture. Thin-layer chromatography was used to track the progress of the reaction. At the end of the reaction, a separating funnel was used to separate the organic components from the reaction mixture using ethyl acetate and brine solution. To remove the residual water molecules, the organic fraction was filtered with anhydrous sodium sulfate. The column chromatography (hexane/ethyl acetate = 10: 1 as the mobile phase and silica 100−200 mesh as the stationary phase) technique was employed to isolate the pure product from the crude organic fraction, which was further used for characterization by ^{1}H NMR and ^{13}C NMR spectroscopy.

3. RESULTS AND DISCUSSION

3.1. X-ray Diffraction (XRD) Studies. The XRD study was undertaken to identify the crystalline phases and to estimate the average crystallite sizes of the as-prepared CeO_2 nanostructures. The XRD pattern in Figure 1 shows the presence of high-intensity peaks at 2θ = 28.6, 33.1, 47.6, 56.4, 59.2, 69.5, 76.7, and 79.1°, which are assigned to (111), (200), (220), (311), (222), (400), (331), and (420) crystal planes, respectively, of the cubic fluorite structure of CeO_2 (JCPDS card #34-0394; space group $Fm\bar{3}m$).[62] The results confirmed the formation of CeO_2 nanostructures of high purity as no other peaks due to any impurity could be detected in the diffractogram. The average crystallite sizes of CeO_2 nanostructures computed using the Debye-Scherer method considering the (111), (220), and (311) reflection planes are 15.6 and 16.4 nm, respectively, for CeO-1 and CeO-2. The lattice parameters were calculated from the XRD data, and the computed value of the lattice constant was 0.54 nm, which matches well with the reported value for CeO_2 nanostructures and bulk CeO_2.[62]

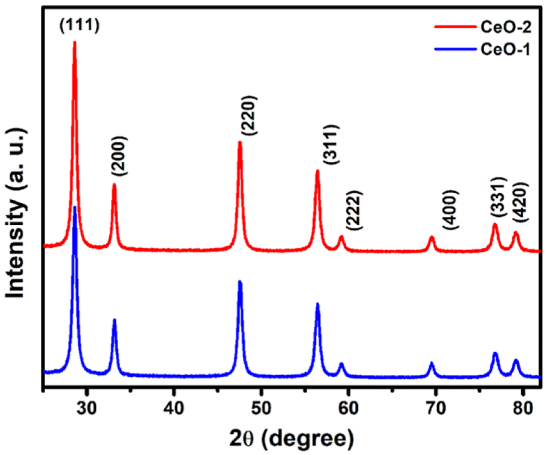

Figure 1. XRD pattern of CeO_2 nanostructures recorded from different samples.

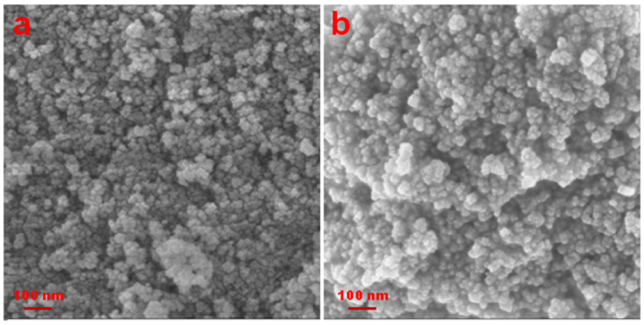

Figure 2. SEM images of samples (a) CeO-1 and (b) CeO-2.

3.2. Electron Microscopy Analysis. Scanning electron microscopy (SEM) was used to investigate the surface topography of the as-prepared CeO_2 nanostructures. The SEM images of CeO-1 and CeO-2 are shown in Figure 2, which shows the formation of smaller-sized particles. However, it is very difficult to understand the morphology and size of the formed particles from the SEM images. Therefore, to understand the morphological evolution and the size of the formed CeO_2 particles, a transmission electron microscopy (TEM) study was undertaken. Figure 3a displays the TEM image of CeO-1, which shows the formation of slightly aggregated cube-shaped CeO_2 nanostructures. The aggregation might be due to the absence of any stabilizer during its growth. The sizes of these cube-shaped CeO_2 nanostructures varied from 11 to 17 nm. The selected area electron diffraction (SAED) pattern (Figure 3b) recorded from CeO-1 indicated the polycrystalline nature of the products. This might be because of the aggregation of the particles on the TEM grid, which causes reflection to take place from multiple particles, forming the ring pattern accompanied by scattered dots on the ring. The high-resolution TEM (HRTEM) image of CeO-1 (Figure 3c) shows that the lattice fringes are perfectly aligned, confirming the formation of well-crystalline CeO_2 nanostructures. The *d*-space value, as calculated using ImageJ software (NIH, USA), is 0.33 nm, which corresponds to the (111) plane in cubic CeO_2 nanostructures. Figure 3d,e shows the TEM image of CeO-2, which also confirms the formation of cube-shaped CeO_2 nanostructures. The sizes of these cube-shaped CeO_2 nanostructures range from 9.5 to 24 nm. The size variation of the formed particles in different samples might be attributed to the different alkali concentrations that control the nucleation rate. The inset in Figure 3f presents the SAED pattern of cube-shaped CeO_2 nanostructures in CeO-2, which again indicated the polycrystalline nature of the products. The perfectly aligned lattice fringes in the HRTEM image of cube-shaped CeO_2 nanostructures in CeO-2 (Figure 3f) also confirm the formation of well-crystalline CeO_2 nanostructures. The *d*-space value calculated using ImageJ software is 0.32 nm, which is again assigned to the (111) plane in CeO_2 nanostructures.

3.3. Optical Properties. UV−vis and room temperature photoluminescence (PL) spectroscopy studies were undertaken to examine the optical behavior of the synthesized CeO_2 nanostructures. Figure 4a displays the UV−vis spectra of CeO_2 nanostructures, which show a high UV absorption characteristic. The maximum absorption peak appeared at around 307 nm, which is blue-shifted compared to that of the bulk CeO_2 (389 nm) and is attributed to the charge transfer between the O 2p states in O^{2-} and Ce 4f states in Ce^{4+}.[63] The observed blue shift in the absorption spectrum of CeO_2 nanostructures might be attributed to the decrease in the size of the particles.[63] The change in the valence state of cerium widens the charge transfer gap between the O 2p and Ce 4f bands as it moves from the +4 to the +3 state, which might also be

https://doi.org/10.1021/acsomega.2c04614
ACS Omega 2022, 7, 42126−42137

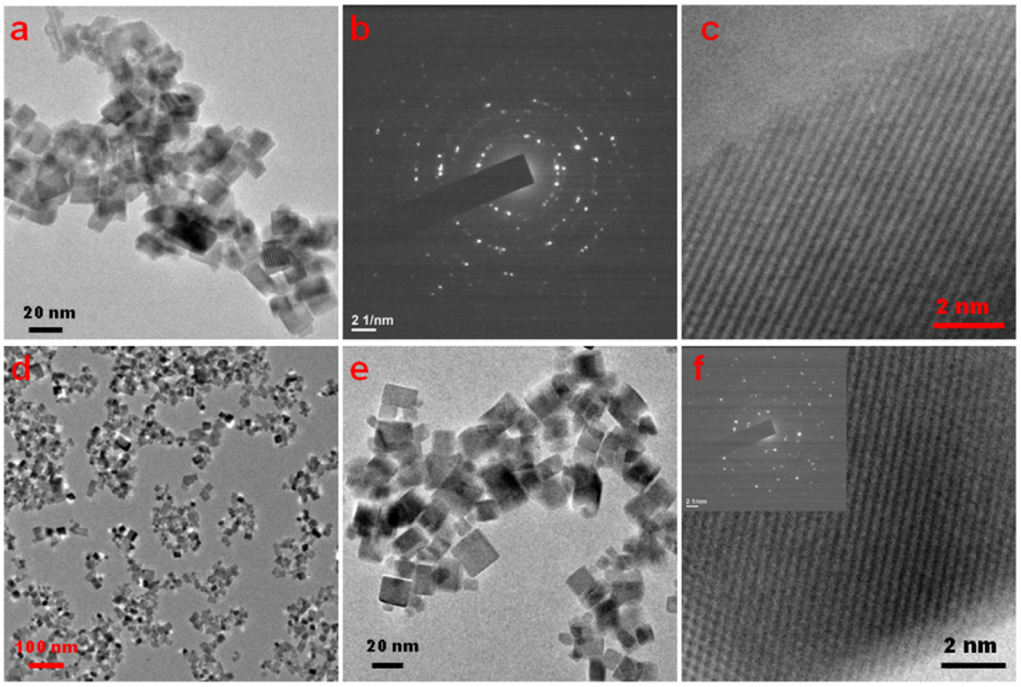

Figure 3. TEM images of CeO_2 nanostructures in (a) CeO-1, (b) SAED pattern of CeO-1, and (c) HRTEM image of CeO-1. (d) Low and (e) high magnification TEM images of CeO-2, and (f) HRTEM image of CeO-2. The inset in Figure 3f represents the SAED pattern of CeO-2.

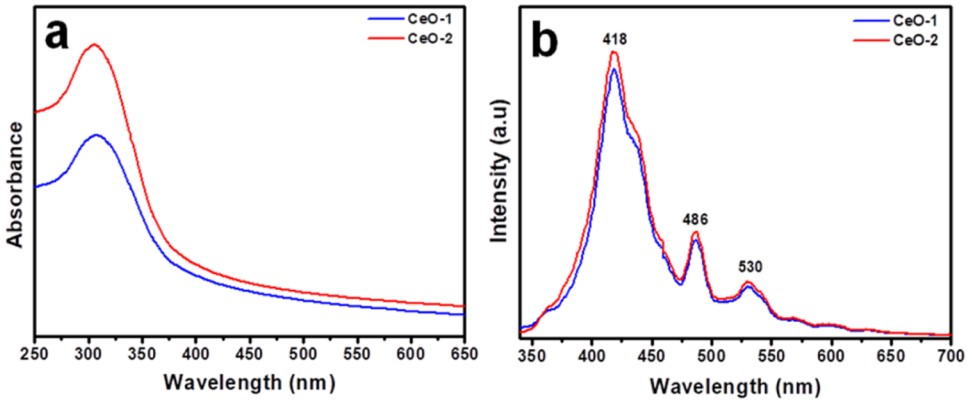

Figure 4. (a) UV−vis absorption and (b) room temperature PL spectra of CeO_2 nanostructures.

responsible for the blue shift in the absorption spectrum of CeO_2 in the nanoscale dimension.[64] The optical band gap in CeO_2 nanostructures, as calculated using the Planck equation is 4.11 eV compared to 3.19 eV in bulk CeO_2. This higher band gap energy is attributed to the nanometer dimension of the particles, as claimed earlier.[65] Figure 4b presents the room temperature PL spectra of CeO_2 nanostructures obtained by exciting the sample at 320 nm. The spectra of both samples exhibit a strong emission peak at 418 nm, which is assumed to originate from the surface defects, while the weak emission band at 486 nm is associated with the relative oxygen vacancies in CeO_2 NPs.[65] The transfer of the charge carrier between the Ce's 4f conduction band and the O's 2p valance band explains the relative oxygen vacancies in CeO_2 NPs.[66] The yellow emission band appeared at 530 nm might be attributed to the interstitial oxygen defects.[65]

3.4. N_2 Gas Adsorption−Desorption Study. Figure 5a shows the N_2 gas adsorption−desorption isotherm of CeO-1, which exhibits a typical IUPAC type IV isotherm with an H3 hysteresis loop, indicating the formation of disordered pore structures with slit-shaped pores, resulting from nonrigid, plate-like CeO_2 particles. Moreover, this kind of hysteresis indicated the presence of a high concentration of mesopores in the material.[67] The Brunauer−Emmett−Teller (BET) surface area of CeO_2 nanostructures (CeO-1), as calculated from the multipoint BET isotherm was found to be 74.1 $m^2\ g^{-1}$, which is much higher than the reported value of 5.67 $m^2\ g^{-1}$ for bulk CeO_2.[68] Moreover, the average pore diameter and volume were calculated from the adsorption−desorption isotherms using the method proposed by Barrett−Joyner−Halenda (BJH). These values are 5.2 nm and 0.136 $cm^3\ g^{-1}$, respectively, confirming that the formed CeO_2 nanostructures are mesoporous. Further, the BJH pore-size distribution curve (inset in Figure 5a) confirms that uniform pores are present in the sample.

3.5. X-ray Photoelectron Spectroscopy Study. X-ray photoelectron spectroscopy (XPS) was used to study the elemental composition and the oxidation state of Ce in the sample. Figure 5b displays the survey scan spectrum of CeO-1, which exhibits the peaks due to Ce 3d and O 1s, confirming

https://doi.org/10.1021/acsomega.2c04614
ACS Omega 2022, 7, 42126−42137

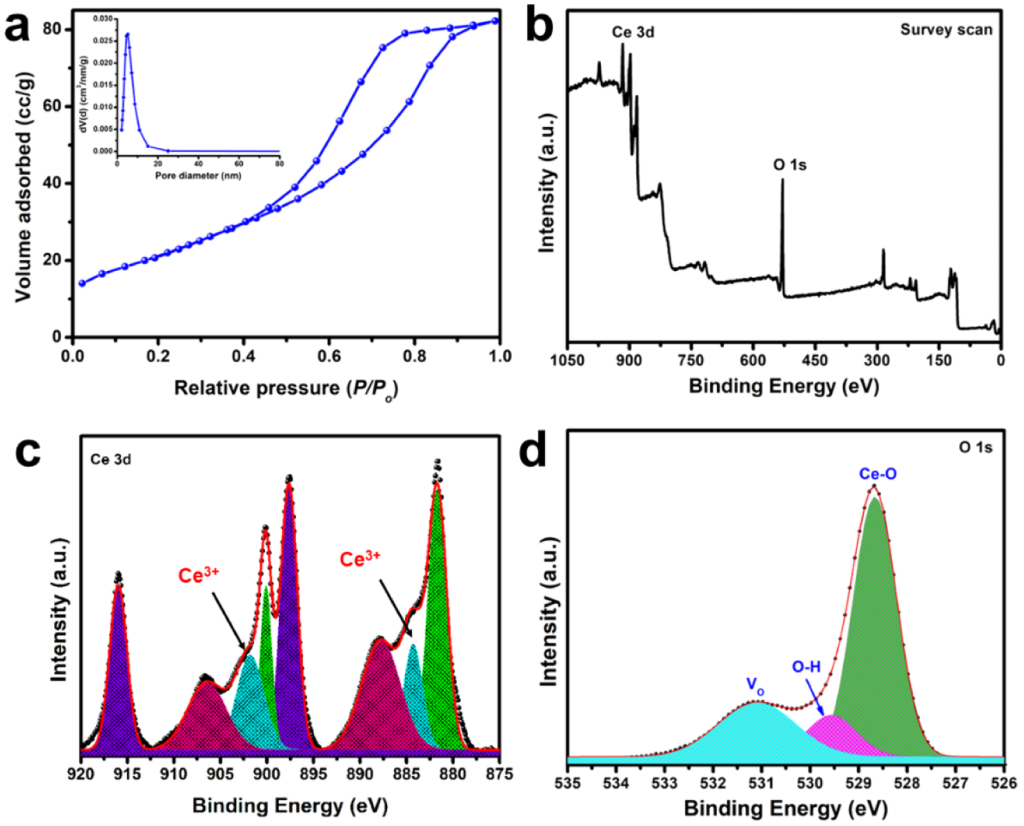

Figure 5. (a) N_2 gas adsorption−desorption isotherm of CeO_2 nanostructures (CeO-1). The inset shows the BJH pore size distribution curve of the same sample. (b) XPS Survey scan spectrum of CeO-1; (c) and (d) are the high-resolution spectra of the Ce 3d and O 1s regions, respectively.

Table 1. Optimization of Reaction Condition for *ipso*-Hydroxylation of Aryl Boronic Acid

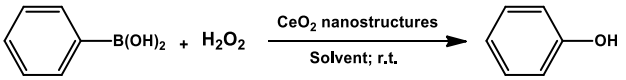

entry	catalyst amount (mg)	30% aq. H_2O_2 (mL)	solvent (3.0 mL)	time (min)	yield[a] (%)
1		2.0	H_2O	60	50
2	15	2.0	H_2O	5	90
3	15	1.0	H_2O	5	90
4	15	0.5	H_2O	5	90
5	15	0.3	H_2O	5	90
6	15	0.2	H_2O	5	90
7	15	0.2	H_2O + C_2H_5OH (v/v = 1:1)	5	95
8	12	0.2	H_2O + C_2H_5OH (v/v = 1:1)	5	95
9	10	0.2	H_2O + C_2H_5OH (v/v = 1:1)	5	95
10	9	0.2	H_2O + C_2H_5OH (v/v = 1:1)	5	90

[a]Isolated yield.

Table 2. Optimization of Reaction Condition for *ipso*-Hydroxylation of Aryl Boronic Acid Under Ultrasonic Vibration[a]

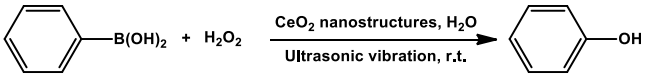

entry	catalyst amount (mg)	30% aq. H_2O_2 (mL)	time (min)	yield[b] (%)
1	10	0.20	5	99
2	8	0.20	5	99
3	7	0.20	5	99
4	6	0.20	5	85
5	7	0.18	5	99
6	7	0.15	5	99
7	7	0.13	5	99
8	7	0.12	5	90
9		0.13	10	40

[a]Reaction condition: phenylboronic acid (1 mmol), H_2O (3.0 mL), and catalyst (CeO-1). [b]Isolated yield.

that the sample consists of Ce, and O. The fitted high-resolution spectrum of the 3d region (Figure 5c) shows the presence of six characteristics peaks for Ce^{4+} in the sample. The peaks centred at 916, 906.5, and 900.2 eV are attributed to $3d_{3/2}$, while the peaks at 897.6, 887.9, and 881.6 eV are due to $3d_{5/2}$ states for Ce^{4+} ions.[69] Additionally, the presence of peaks at 901.9 and 884.3 eV further confirms that Ce^{3+} is also present in the sample.[69] This confirms that Ce exists in the mixed-valence state of +3 and +4 in the product, which is a very common phenomenon. Figure 5d presents the fitted high-resolution spectrum of the O 1s region, which reveals the presence of a strong peak at 528.7 eV due to the presence of lattice oxygen in the O^{2-} state in the product.[70] The weakly intense peak observed at 529.5 eV is assigned to the −OH group from adsorbed moisture, while the broad peak at 531.1 eV corresponds to the oxygen vacancy (V_O) in the sample.[71]

3.6. *Ipso*-hydroxylation of Aryl Boronic Acid. To investigate the catalytic efficiency of the as-prepared CeO_2 nanostructures, the *ipso*-hydroxylation of aryl boronic acid was

https://doi.org/10.1021/acsomega.2c04614
ACS Omega 2022, 7, 42126−42137

Table 3. Substrate Scope for *ipso*-Hydroxylation of Phenylboronic Acid Under Ultrasonic Vibration[a]

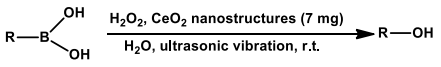

Entry	R–	Time (min)	Yield[b] (%)
1		5	99
2	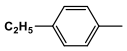	5	99
3	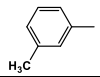	5	99
4	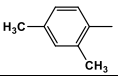	7	99
5	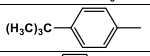	7	95
6	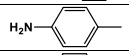	5	99
7	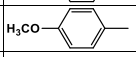	5	95
8	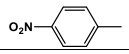	10	90
9		10	85
10	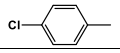	7	96

[a]Reaction condition: aryl boronic acid (1.0 mmol), H_2O_2 (0.13 mL), H_2O (3.0 mL), and catalyst (CeO-1). [b]Isolated yield.

Table 4. Optimization of Reaction Conditions for the aza-Michael Reaction Under Ultrasonic Vibration[a]

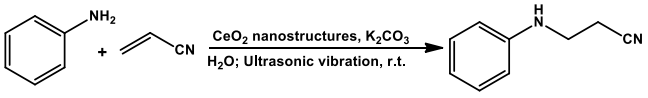

entry	catalyst amount (mg)	K_2CO_3 (mg)	time (h)	yield[b] (%)
1			4	25
2	15		3	60
3	20		3	60
4	15	139	2	87[c]
5	15	69	2	91
6	15	50	2	91
7	15	45	2	80
8		50	2	50
9	12	50	2	91
10	10	50	2	91
11	8	50	2	83
12	10	50	4	60[d]

[a]Reaction condition: aniline (1 mmol) diluted in 0.5 mL of ethanol, acrylonitrile (2.5 mmol), and H_2O (3.0 mL). [b]Isolated yield. [c]Small amount of by-product formed. [d]The reaction was carried under magnetic stirring at 45 °C.

chosen as the standard reaction. For the initial investigation, 1.0 mmol phenylboronic acid was dissolved in 3.0 mL of water taken in a 25 mL round bottom flask under constant stirring. To this solution; 2.0 mL of H_2O_2 (30% aq.) was added, and the reaction progress was tracked by thin-layer chromatography (TLC). We observed a poor yield of 50% after 1.0 h of reaction (Table 1; entry 1). The addition of a small amount of CeO_2 nanostructures (15.0 mg; CeO-1) under identical reaction conditions improved the product yield significantly in 5.0 min (Table 1; entry 2). In the next step, the volume of H_2O_2 (30% aq.) was decreased continuously in the new batches of similar reactions with the fixed amount of the catalyst (15.0 mg) (Table 1; entries 3−6). It was observed that 0.2 mL of H_2O_2 (30% aq.) is enough to bring about a 90% product yield (Table 1; entry 6). We recorded a maximum yield of the product in a mixture of ethanol and water (1:1; v/v) (Table 1; entry 7), which might be due to the enhanced solubility of phenylboronic acid in the solvent mixture. Therefore, considering the ethanol−water mixture (1:1; v/v) as the best solvent system, we continuously decreased the amount of catalyst under identical reaction conditions and observed a very satisfactory yield of 95% using 10.0 mg of CeO_2 nanostructures (CeO-1) and 0.2 mL of H_2O_2 (30% aq.) within 5.0 min (Table 1; entry 9). We also observed a similar product yield with the other catalyst (CeO-2). When the *ipso*-hydroxylation was carried out under ultrasonic vibration maintaining all other reaction conditions identical, the yield of the product was surprisingly increased to 99% (Table 2; entry 1). Therefore, to further check if similar results can be obtained with a lower amount of catalyst under ultrasonic vibration, we repeated the reaction with different catalyst loadings. We were happy to note that 7.0 mg of CeO_2 nanostructures is enough to furnish 99% yield in 5 min (Table 2; entry 3). Moreover, while optimizing the amount of H_2O_2 (Table 2; entries 5−8), it was observed that 0.13 mL of H_2O_2 is enough to produce a 99% yield with 7.0 mg of CeO_2 nanostructures in 5.0 min (Table 2; entry 7). It is to be noted that under ultrasonic vibration, the addition of ethanol is not necessary, unlike in the mechanical stirring discussed above. Without the presence of the catalyst, only a 40% yield of the product could be obtained within 10.0 min under ultrasonic vibration (Table 2; entry 9). We also noticed that both the CeO-1 and CeO-2 produced an identical yield of the product under identical reaction conditions. However, the use of commercial CeO_2 significantly decreased the product yield to 55% under the same reaction conditions. This signifies the importance of the cube-shaped CeO_2 NPs in the *ipso*-hydroxylation of aryl boronic acid. Based on the above-mentioned observations, CeO-1 was chosen for further investigation.

To investigate the substrate scope and constraints of the newly developed procedure, different substituted aryl boronic acids were examined utilizing CeO_2 nanostructures (CeO-1) under ultrasonic vibration (Table 3). It was observed that the position and the type of substituted groups had slightly altered the reaction time and yield of the products. The *meta*- and *para*-substituted aryl boronic acids with electron-donating groups provided an excellent yield (Table 3; entries 2 and 3). However, the presence of the $-CH_3$ group at the ortho position of 4-methyl phenylboronic acid slightly slowed down the reaction rate without compromising the product yield (Table 3; entry 4), which might be due to the *ortho* effect. Further, we observed a slightly decreased product yield with the para-substituted aryl boronic acids with electron-donating bulky groups (Table 3; entry 5). Moreover, the protocol offered a good yield, taking more reaction time for electron-withdrawing groups and electronegative heteroatom in the structure of phenylboronic acids (Table 3; entries 7, 8, 9, and 10).

3.7. aza-Michael Reaction. After the successful utilization of CeO_2 nanostructures as a catalyst in the *ipso*-hydroxylation of different substituted phenylboronic acids, we wanted to see the versatility of the catalyst for use in the aza-Michael reaction

https://doi.org/10.1021/acsomega.2c04614
ACS Omega 2022, 7, 42126−42137

Table 5. Substrate Scope for the aza–Michael Reaction Under Ultrasonic Vibration[a]

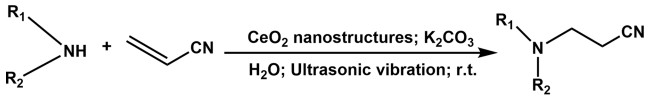

R_1 = alkyl, aryl, benzyl
R_2 = -H, alkyl

Entry	Amines	Product	Time (min)	Yield[b] (%)
1	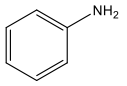	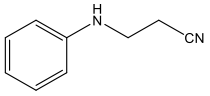	120	91
2	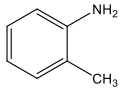	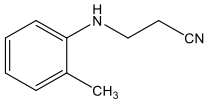	120	80
3	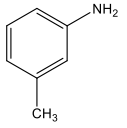	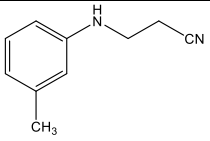	120	92
4	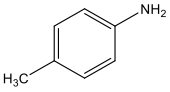	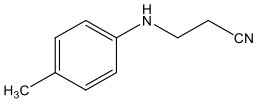	120	92
5	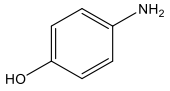	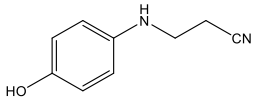	120	87
6	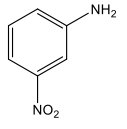	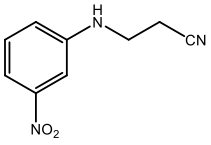	120	30
7	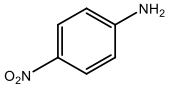	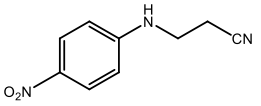	120	trace
8	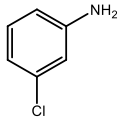	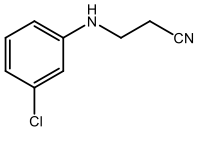	120	80
9	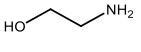	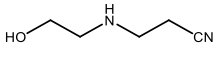	80	60
10	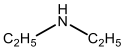	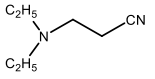	120	90
11	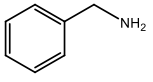	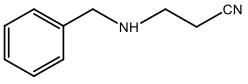	120	80

[a]Reaction condition: amine (1 mmol) diluted in 0.5 mL of ethanol, acrylonitrile (2.5 mmol), and H_2O (3.0 mL). [b]Isolated yield.

https://doi.org/10.1021/acsomega.2c04614
ACS Omega 2022, 7, 42126–42137

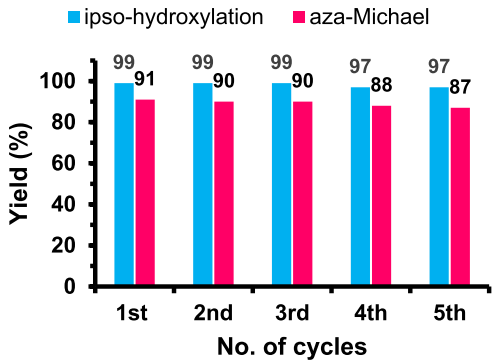

Figure 6. Bar diagram showing recycling data of the catalyst in the *ipso*-hydroxylation and aza-Michael reactions.

with acrylonitrile acting as the Michael acceptor. We performed the preliminary study with 1.0 mmol aniline and 2.5 mmol acrylonitrile in 3.0 mL of water as the solvent without adding any catalyst and base under ultrasonic vibration at room temperature (Table 4; entry 1). We observed a very poor yield of ∼25% after 4.0 h. It is to be noted that the required amount of aniline was diluted with 0.5 mL of ethanol to enhance the solubility of aniline. When the reaction was repeated with 15.0 mg of CeO_2 nanostructures (CeO-1) as the catalyst, the yield of the product improved significantly after 3.0 h (Table 4; entry 2). In another experiment, we increased the catalyst loading to 20.0 mg, but the yield of the product was not improved further (Table 4; entry 3). Therefore, we added K_2CO_3 (139.0 mg) to the reaction mixture containing 15 mg of the catalyst to see if any improvement in the product yield could be observed. We were delighted to note that the yield of the product increased significantly within 2.0 h but with the formation of some by-products, which might be due to the double substitution of the nitrogen atom of aniline (Table 4; entry 4). Therefore, in the next step, 69.0 mg of K_2CO_3 (0.5 equivalent) was added, keeping all other reaction parameters identical. Surprisingly, we noticed an increase in the product yield without any additional by-products (Table 4; entry 5). After a systematic study, it was observed that 50 mg of K_2CO_3 is enough to furnish a 91% yield with the same amount of the catalyst (CeO-1, 15.0 mg) (Table 4; entries 6 and 7). However, when we performed the reaction without a catalyst but with the base K_2CO_3 (50.0 mg), the yield of the product decreased sharply, which indicates the necessity of the catalyst (Table 4; entry 8). Furthermore, to optimize for the catalyst loading, we varied the amount of catalyst under identical reaction conditions (Table 4; entry 9−11), and we observed that 10.0 mg of CeO_2 nanostructures (CeO-1) are sufficient to furnish a maximum of 91% product yield in 2.0 h (Table 4; entry 10). Additionally, when the aza-Michael reaction was repeated at 45 °C under mechanical stirring, only a 60% product yield was recorded after 4.0 h (Table 4; entry 12). Moreover, similar results were obtained when CeO-1 was replaced by CeO-2. The similar catalytic activity of both CeO-1 and CeO-2 is attributed to the similarity in their morphologies and surface characteristics. In a controlled experiment, when we used the commercial CeO_2, the product yield of the addition reaction was significantly decreased to 60% under identical reaction conditions. This signifies that the size, shape, and surface properties of the catalyst are vital for excellent product yield. Although the aza-Michael reaction involving amines and acrylonitrile is spontaneous, the rate of the reaction is very slow, as observed by many researchers. Therefore, alkaline conditions and the requirement of an acidic catalyst are necessary to make this type of conjugated addition faster.[72] According to a previous report, the presence of K_2CO_3 with the MgO catalyst enhanced the rate of reaction between amines and electron-deficient alkenes due to the formation of stronger active sites on the MgO surface because of the strong interaction between K_2CO_3 and MgO.[72] In the present study, the driving force of the proposed aza-Michael reaction might be a result of the combined effect of ultrasonic vibration, K_2CO_3 and CeO_2 nanostructures. We believe that, in the current study, K_2CO_3 behaves as an electrolyte, which produces CO_3^{2-} ions that get selectively adsorbed on the surface of CeO_2 nanostructures and thereby create active sites for the reactions. Moreover, the Ce^{3+}/Ce^{4+} redox couple present on the surface of CeO_2 helps Ce^{4+} sites to undergo easy conversion into Ce^{3+} via coordination with carbonate ions, forming $Ce-O-CO_2H$, which is believed to be activated acrylonitrile for the reaction.[3] The application of ultrasound in combination with K_2CO_3 might also provide the required activation energy for the reaction, where ultrasound alone could not accelerate the progress of the reaction.

To investigate the substrate scope and constraints of the newly developed protocol, several substituted anilines and aliphatic amines (Table 5) were examined, which gave

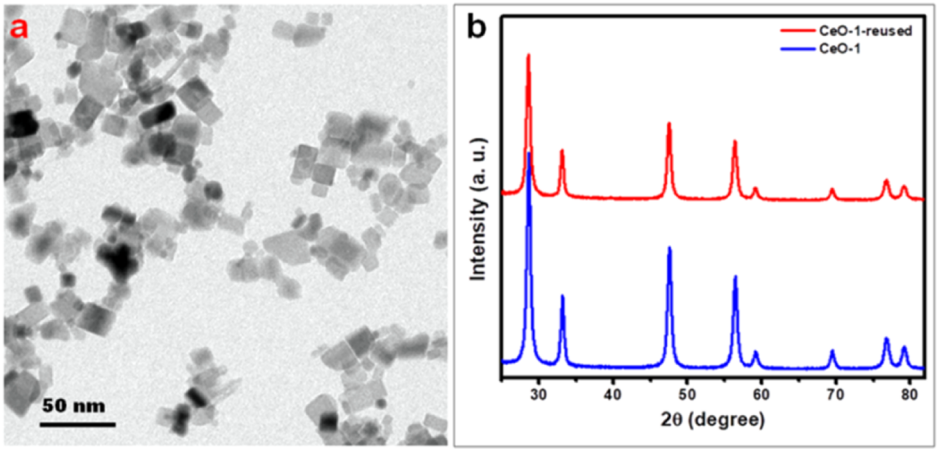

Figure 7. (a) TEM image and (b) XRD pattern of the reused sample (CeO-1).

https://doi.org/10.1021/acsomega.2c04614
ACS Omega 2022, 7, 42126−42137

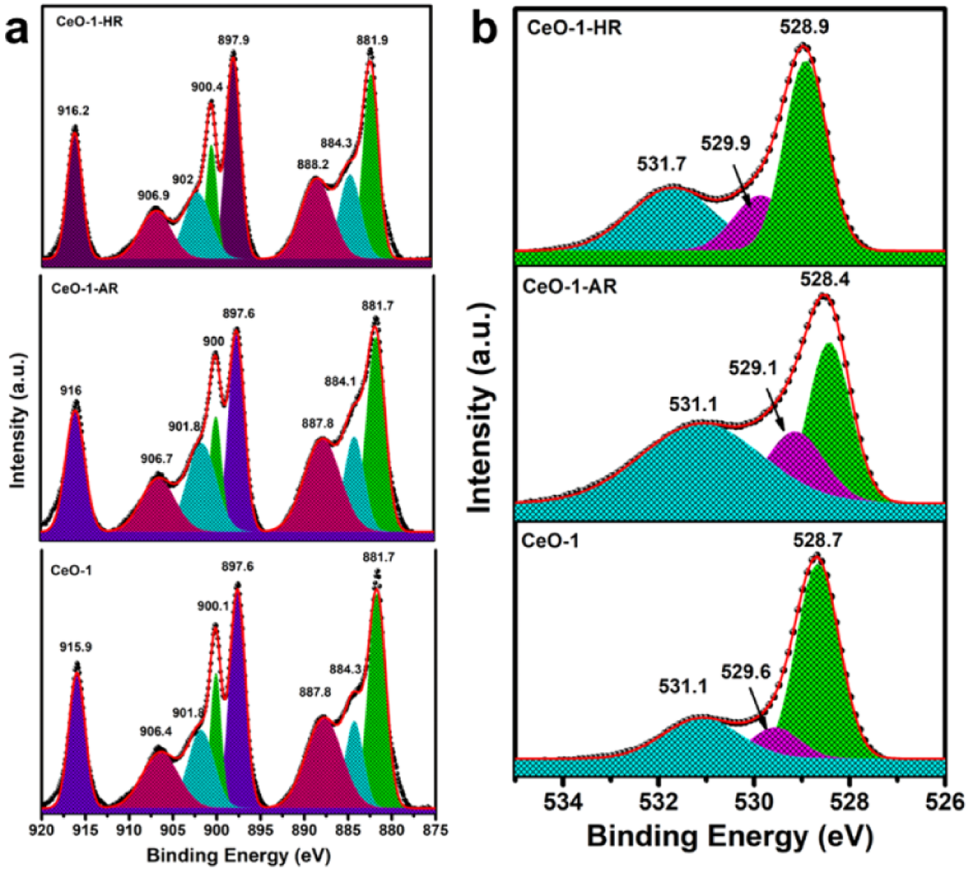

Figure 8. Fitted curves of (a) Ce 3d and (b) O 1s region of CeO-1 before and after catalysis. CeO-1 is the nascent catalyst, and CeO-1AR and CeO-1HR are used samples in the aza-Michael and *ipso*-hydroxylation reactions.

moderate to excellent yields. However, we observed an improved yield of the product when the amine was substituted at the *meta* and *para* positions with an electron-donating group, due to the positive inductive effect (Table 5; entries 3 and 4). However, the product yield was decreased, when the amine was substituted with an electron-donating group at the *ortho* position due to the steric hindrance (Table 5; entry 2). Moreover, the electron-withdrawing groups decrease the product yield significantly due to the negative inductive effect and negative resonance effect (Table 5; entries 5−8). The reason for the low yield in the case of aliphatic amine (ethanolamine) might be due to the high degree of solvation of the smaller Michael donor ethanolamine, where two polar groups −OH and $-NH_2$ are present (Table 5; entry 9). However, a better yield was obtained from diethylamine, which was less readily solvated by the polar solvent than ethanolamine (Table 5; entry 10). Another possibility might be the differences in the nucleophilicity of primary and secondary amines. Furthermore, a comparatively low yield was obtained from benzylamine as a Michael donor, which might be due to the inappropriate solubility and low nucleophilicity of the reactant benzylamine in the studied solvent (Table 5; entry 11).

3.8. Reusability of CeO_2 Nanostructures. The stability and reusability of a heterogeneous catalyst are vital for its potential application for commercial purposes. To assess the stability and reusability of CeO_2 nanostructures in both the *ipso*-hydroxylation reaction and the aza-Michael reaction, we isolated the used CeO_2 nanostructures (CeO-1) from the aqueous fraction after the catalysis reaction by centrifugation, followed by three cycles of washing using ethanol to remove any trace of surface-adsorbed organic components. The recovered catalyst was then dried under a vacuum at 60 °C overnight and reused in fresh batches of the *ipso*-hydroxylation reaction and the aza-Michael reaction separately. We observed that CeO_2 nanostructures can be reused up to the fifth cycle with a minimal loss of activity in both the *ipso*-hydroxylation reaction and the aza-Michael reaction (Figure 6). We believe that the possible adsorption of either the reactants or the products on the catalyst's surface is responsible for such a slight decrease in the catalytic activity of CeO_2 nanostructures. Further, the fate of the used catalyst was examined by XRD, XPS, and TEM studies. It was observed from Figure 7 that no morphological change of the CeO_2 nanostructures took place due to catalysis. Also, the phase structure, as well as the crystalline property, remained intact after the catalysis. Besides, no significant change in the characteristic peak positions due to Ce3d and O1s was observed after the catalysis reaction (Figure 8). It can be inferred that these catalysts are stable enough under the experimental conditions and are suitable for further use in successive batches of catalysis.

4. CONCLUSIONS

In this study, we demonstrated the synthesis of cube-shaped CeO_2 nanostructures by the hydrothermal method without using any added template or surfactant. These cube-shaped CeO_2 nanostructures are pure, well-crystalline, and possess a cubic fluorite structure. The as-synthesized CeO_2 nanostructures act as excellent catalysts in the *ipso*-hydroxylation

https://doi.org/10.1021/acsomega.2c04614
ACS Omega 2022, 7, 42126−42137

reaction of aryl boronic acids and the aza-Michael reaction involving aromatic or aliphatic amines with acrylonitrile at room temperature under ultrasonic vibration. In the CeO_2-catalyzed *ipso*-hydroxylation reaction, the requirement of hydrogen peroxide is very low compared to many of the recent literature reports, so the use of CeO_2 nanostructures in the *ipso*-hydroxylation reaction could be a greener synthetic route for large scale synthesis. Also, the proposed protocol involving the CeO_2 nanostructures, which catalyzed the aza-Michael reaction under ultrasonic vibration, is more effective than some of the supported catalysts that require high temperatures, harsh solvents, strong bases, ligands, and long reaction times. The stability and reusability potential of the catalysts in both the studied reactions provide additional advantages for their future application in industrial use.

■ ASSOCIATED CONTENT

Supporting Information

The Supporting Information is available free of charge at https://pubs.acs.org/doi/10.1021/acsomega.2c04614.

Characterization of the catalyst and catalyzed products and relevant ^1H and ^{13}C NMR spectra of different products (PDF)

■ AUTHOR INFORMATION

Corresponding Author

Md. Harunar Rashid − *Department of Chemistry, Rajiv Gandhi University, Doimukh 791112 Arunachal Pradesh, India;* orcid.org/0000-0001-7470-8384; Email: harunar.rashid@rgu.ac.in

Authors

Tulan Chandra Saikia − *Department of Chemistry, Rajiv Gandhi University, Doimukh 791112 Arunachal Pradesh, India;* orcid.org/0000-0002-7457-8126

Xavy Borgohain − *Department of Chemistry, Rajiv Gandhi University, Doimukh 791112 Arunachal Pradesh, India*

Saddam Iraqui − *Department of Chemistry, Rajiv Gandhi University, Doimukh 791112 Arunachal Pradesh, India*

Complete contact information is available at: https://pubs.acs.org/10.1021/acsomega.2c04614

Author Contributions

T.C.S., X.B., and S.I. contributed equally. Tulan Chandra Saikia: conceptualization, methodology, formal analysis, and original draft preparation. Xavy Borgohain: catalyst preparation and formal analysis. Saddam Iraqui: catalysis experiment and investigation. Md. Harunar Rashid: supervision, conceptualization, review, and editing. All authors reviewed the manuscript.

Notes

The authors declare no competing financial interest.

■ ACKNOWLEDGMENTS

We acknowledge the Department of Science and Technology, Government of India, for partially supporting the research under the DST-PURSE programme (SR/PURSE/2021/58). The authors thank CSIR-NEIST Jorhat, SAIC TU, CNN-JMI, and SAIF-GU for providing instrumental facilities to us.

■ REFERENCES

(1) Gad, S. C. *Cerium*. In *Encyclopedia of Toxicology* 2ed.; Wexler, P., Eds.; Elsevier, 2005; pp 502-503.

(2) Koskenmaki, D. C.; Gschneidner, K. A.. *Cerium*; Elsevier, 1978; Vol. *1*, pp 337−377.*Handbook on the Physics and Chemistry of Rare Earths*

(3) Piro, N. A.; Robinson, J. R.; Walsh, P. J.; Schelter, E. J. The electrochemical behavior of cerium(III/IV) complexes: Thermodynamics, kinetics and applications in synthesis. *Coord. Chem. Rev.* **2014**, *260*, 21−36.

(4) Younis, A.; Chu, D.; Li, S. *Cerium Oxide Nanostructures and their Applications*. In *Functionalized Nanomaterials*; Farrukh, M. A., Ed.; IntechOpen, 2016.

(5) Tang, W.-X.; Gao, P.-X. Nanostructured cerium oxide: preparation, characterization, and application in energy and environmental catalysis. *MRS Commun* **2016**, *6*, 311−329.

(6) Anthony, E. T.; Ojemaye, M. O.; Okoh, A. I.; Okoh, O. O. Synthesis of CeO_2 as promising adsorbent for the management of free-DNA harboring antibiotic resistance genes from tap-water. *Chem. Eng. J.* **2020**, *401*, 125562.

(7) Chaudhary, S.; Sharma, P.; Singh, D.; Umar, A.; Kumar, R. Chemical and pathogenic cleanup of wastewater using surface-functionalized CeO_2 nanoparticles. *ACS Sustain. Chem. Eng.* **2017**, *5*, 6803−6816.

(8) Han, W.-Q.; Wen, W.; Hanson, J. C.; Teng, X.; Marinkovic, N.; Rodriguez, J. A. One-dimensional ceria as catalyst for the low-temperature water−gas shift reaction. *J. Phys. Chem. C* **2009**, *113*, 21949−21955.

(9) Jasinski, P.; Suzuki, T.; Anderson, H. U. Nanocrystalline undoped ceria oxygen sensor. *Sens. Actuators B Chem.* **2003**, *95*, 73−77.

(10) Seong, G.; Dejhosseini, M.; Adschiri, T. A kinetic study of catalytic hydrothermal reactions of acetaldehyde with cubic CeO_2 nanoparticles. *Appl. Catal. A* **2018**, *550*, 284−296.

(11) Skorodumova, N. V.; Simak, S. I.; Lundqvist, B. I.; Abrikosov, I. A.; Johansson, B. Quantum origin of the oxygen storage capability of ceria. *Phys. Rev. Lett.* **2002**, *89*, 166601.

(12) Xie, W.; Liu, B.; Xiao, S.; Li, H.; Wang, Y.; Cai, D.; Wang, D.; Wang, L.; Liu, Y.; Li, Q.; et al. High performance humidity sensors based on CeO_2 nanoparticles. *Sens. Actuators B: Chem.* **2015**, *215*, 125−132.

(13) Zheng, N.-C.; Wang, Z.; Long, J.-Y.; Kong, L.-J.; Chen, D.-Y.; Liu, Z.-Q. Shape-dependent adsorption of CeO_2 nanostructures for superior organic dye removal. *J. Colloid Interface Sci.* **2018**, *525*, 225−233.

(14) Trovarelli, A.; de Leitenburg, C.; Boaro, M.; Dolcetti, G. The utilization of ceria in industrial catalysis. *Catal. Today* **1999**, *50*, 353−367.

(15) Singh, K. R. B.; Nayak, V.; Sarkar, T.; Singh, R. P. Cerium oxide nanoparticles: properties, biosynthesis and biomedical application. *RSC Adv.* **2020**, *10*, 27194−27214.

(16) Tundo, P.; Griguol, E. Green chemistry for sustainable development. *Chem. Int.* **2018**, *40*, 18−24.

(17) Doble, M.; Kruthiventi, A. K. *Alternate Solvents*. In *Green Chemistry and Engineering*; Doble, M., Kruthiventi, A. K., Eds.; Academic Press, 2007, pp 93−104

(18) Lim, F. P. L.; Dolzhenko, A. V. *Atom economy in green organic synthesis*. In *Green Sustainable Process for Chemical and Environmental Engineering and Science*; Inamuddin, Boddula, R., Asiri, A. M., Eds.; Elsevier, 2020, pp 1−12.

(19) Thomas, J. M.; Raja, R. Designing catalysts for clean technology, green chemistry, and sustainable development. *Ann. Rev. Mater. Res.* **2005**, *35*, 315−350.

(20) Akbayrak, S.; Özkar, S. Supported nanoparticles for liquid-phase catalysis.. In *Encyclopedia of Interfacial Chemistry*; Wandelt, K., Ed.; Elsevier, 2018, pp 607−624.*Supported Nanoparticles for Liquid-Phase Catalysis* DOI: 10.1016/b978-0-12-409547-2.12999-3

(21) Deyris, P.-A.; Grison, C. Nature, ecology and chemistry: An unusual combination for a new green catalysis, ecocatalysis. *Curr. Opin. Green Sustain. Chem.* **2018**, *10*, 6−10.

(22) *Polyhydric phenols*. In *Studies in Organic Chemistry*, Tyman, J. H. P., Ed.; Vol. *52*; Elsevier, 1996; pp 338-357.

(23) Liang, H.; Ciufolini, M. A. Biomimetic Synthesis of Alkaloids Derived from Tyrosine: The Case of FR-901483 and TAN-1251 Compounds. *Biomimetic Organic Synthesis*, 2011, pp 61−89.
(24) Castro-Godoy, W. D.; Schmidt, L. C.; Argüello, J. E. A Green Alternative for the conversion of arylboronic acids/esters into phenols promoted by a reducing agent, sodium sulfite. *Eur. J. Org. Chem.* **2019**, *2019*, 3035−3039.
(25) Chen, G.; Chan, A. S. C.; Kwong, F. Y. Palladium-catalyzed C-O bond formation: direct synthesis of phenols and aryl/alkyl ethers from activated aryl halides. *Tetrahedron Lett.* **2007**, *48*, 473−476.
(26) Ghaffarzadeh, M.; Bolourtchian, M.; Hosseini, M. R.; Hosseini, M. Synthesis of phenols and naphthols by alkali metal hydroxide fusion under microwave irradiation. *J. Chem. Res.* **2003**, *2003*, 812−813.
(27) Fortuin, J. P.; Waterman, H. I. Production of phenol from cumene. *Chem. Eng. Sci.* **1953**, *2*, 182−192.
(28) Cohen, T.; Dietz, A. G.; Miser, J. R. A simple preparation of phenols from diazonium ions via the generation and oxidation of aryl radicals by copper salts. *J. Org. Chem.* **1977**, *42*, 2053−2058.
(29) Bartolomei, B.; Gentile, G.; Rosso, C.; Filippini, G.; Prato, M. Turning the light on phenols: New opportunities in organic synthesis. *Chem. Eur. J.* **2021**, *27*, 16062−16070.
(30) Mahanta, A.; Chandra Saikia, T.; Bharali, S. J. Titanium dioxide as an efficient heterogeneous catalyst for quick C-B bond cleavage of aryl/hetero arylboronic acid on water at room temperature. *Sustain. Chem. Pharm.* **2020**, *18*, 100301.
(31) Mondal, M.; Bora, U. An efficient protocol for palladium-catalyzed ligand-free Suzuki−Miyaura coupling in water. *Green Chem.* **2012**, *14*, 1873−1876.
(32) Prakash, G. K. S.; Chacko, S.; Panja, C.; Thomas, T. E.; Gurung, L.; Rasul, G.; Mathew, T.; Olah, G. A. Regioselective synthesis of phenols and halophenols from arylboronic acids using solid poly(N-vinylpyrrolidone)/ hydrogen peroxide and poly(4-vinylpyridine)/hydrogen peroxide complexes. *Adv. Synth. Catal.* **2009**, *351*, 1567−1574.
(33) Zhu, C.; Wang, R.; Falck, J. R. Mild and rapid hydroxylation of aryl/heteroaryl boronic acids and boronate esters with N-oxides. *Org. Lett.* **2012**, *14*, 3494−3497.
(34) Chatterjee, N.; Goswami, A. Organic hypervalent iodine(III) catalyzed*ipso*-hydroxylation of aryl- and alkylboronic acids/esters. *Tetrahedron Lett.* **2015**, *56*, 1524−1527.
(35) Begum, T.; Gogoi, A.; Gogoi, P. K.; Bora, U. Catalysis by mont K-10 supported silver nanoparticles: a rapid and green protocol for the efficient *ipso*-hydroxylation of arylboronic acids. *Tetrahedron Lett.* **2015**, *56*, 95−97.
(36) Kandula, V.; Nagababu, U.; Behera, M.; Yennam, S.; Chatterjee, A. A facile green synthesis of silver nanoparticles: An investigation on catalytic hydroxylation studies for efficient conversion of aryl boronic acids to phenol. *J. Saudi Chem. Soc.* **2019**, *23*, 711−717.
(37) Karthik, M.; Suresh, P. Graphene oxide as a carbocatalyst for sustainable *ipso*-hydroxylation of arylboronic acids: A simple and straightforward strategy to access phenols. *ACS Sustain. Chem. Eng.* **2019**, *7*, 9028−9034.
(38) Borah, R.; Saikia, E.; Bora, S. J.; Chetia, B. On-water synthesis of phenols using biogenic Cu_2O nanoparticles without using H_2O_2. *RSC Adv.* **2016**, *6*, 100443−100447.
(39) Phukan, S.; Mahanta, A.; Rashid, M. H. Size-tunable ZnO nanotapes as an efficient catalyst for oxidative chemoselective C-B bond cleavage of arylboronic acids. *Appl. Catal. A* **2018**, *562*, 58−66.
(40) Saikia, T. C.; Iraqui, S.; Rashid, M. H. Synergistic effect of PEG-coated ZnO nanoparticles and ultrasonic irradiation on the C-B bond cleavage of aryl boronic acids. *Sustain. Chem. Pharm.* **2022**, *25*, 100613.
(41) Saikia, I.; Hazarika, M.; Hussian, N.; Das, M. R.; Tamuly, C. Biogenic synthesis of Fe_2O_3@SiO_2 nanoparticles for *ipso*-hydroxylation of boronic acid in water. *Tetrahedron Lett.* **2017**, *58*, 4255−4259.
(42) Das, S. K.; Tahu, M.; Gohain, M.; Deka, D.; Bora, U. Bio-based sustainable heterogeneous catalyst for *ipso*-hydroxylation of arylboronic acid. *Sustain. Chem. Pharm.* **2020**, *17*, 100296.
(43) Gogoi, A.; Bora, U. A mild and efficient protocol for the *ipso*-hydroxylation of arylboronic acids. *Tetrahedron Lett.* **2013**, *54*, 1821−1823.
(44) Atia, A. A.; Kimura, M. Oxidative hydroxylation of aryl boronic acid catalyzed by co-porphyrin complexes via blue-light irradiation. *Catalysts* **2020**, *10*, 1262.
(45) Amara, Z.; Caron, J.; Joseph, D. Recent contributions from the asymmetric aza-Michael reaction to alkaloids total synthesis. *Nat. Prod. Rep.* **2013**, *30*, 1211−1225.
(46) Chowdhury, R.; Khan, A.; Rashid, M. H. Green synthesis of CuO nanoparticles using *Lantana camara* flower extract and their potential catalytic activity towards the aza-Michael reaction. *RSC Adv.* **2020**, *10*, 14374−14385.
(47) Rulev, A. Y. aza-Michael reaction: achievements and prospects. *Russ. Chem. Rev.* **2011**, *80*, 197−218.
(48) Saikia, T. C.; Iraqui, S.; Khan, A.; Rashid, M. H. *Sapindus mukorossi* seed shell extract mediated green synthesis of CuO nanostructures: an efficient catalyst for C-N bond-forming reactions. *Mater. Adv.* **2022**, *3*, 1115−1124.
(49) Ranu, B. C.; Banerjee, S. Significant rate acceleration of the aza-Michael reaction in water. *Tetrahedron Lett.* **2007**, *48*, 141−143.
(50) Verma, S.; Jain, S. L.; Sain, B. An efficient biomaterial supported bifunctional organocatalyst ($ES\text{-}SO_3\text{-}C_5H_5NH^+$) for the synthesis of β-amino carbonyls. *Org. Biomol. Chem.* **2011**, *9*, 2314−2318.
(51) De, K.; Legros, J.; Crousse, B.; Bonnet-Delpon, D. Solvent-promoted and -controlled aza-Michael reaction with aromatic amines. *J. Org. Chem.* **2009**, *74*, 6260−6265.
(52) Saidi, M. R.; Pourshojaei, Y.; Aryanasab, F. Highly efficient Michael addition reaction of amines catalyzed by silica-supported aluminum chloride. *Synth. Commun.* **2009**, *39*, 1109−1119.
(53) Li, Z.-X.; Luo, D.; Li, M.-M.; Xing, X.-F.; Ma, Z.-Z.; Xu, H. Recyclable Fe_3O_4 nanoparticles catalysts for aza-Michael addition of acryl amides by magnetic field. *Catalysts* **2017**, *7*, 219.
(54) Liu, X.; Lu, M.; Gu, G.; Lu, T. aza-Michael reactions in water using functionalized ionic liquids as the recyclable catalysts. *J. Iran. Chem. Soc.* **2011**, *8*, 775−781.
(55) Roy, S. R.; Chakraborti, A. K. Supramolecular assemblies in ionic liquid catalysis for aza-Michael reaction. *Org. Lett.* **2010**, *12*, 3866−3869.
(56) Bhattacharjee, S.; Shaikh, A. A.; Ahn, W.-S. Heterogeneous aza-Michael addition reaction by the copper-based metal−organic framework (CuBTC). *Catal. Lett.* **2021**, *151*, 2011−2018.
(57) Nguyen, L. T. L.; Nguyen, T. T.; Nguyen, K. D.; Phan, N. T. S. Metal-organic framework MOF-199 as an efficient heterogeneous catalyst for the aza-Michael reaction. *Appl. Catal. A* **2012**, *425-426*, 44−52.
(58) Yang, J.; Li, T.; Zhou, H.; Li, N.; Xie, D.; Li, Z. Potassium hydroxide catalysed intermolecular aza-Michael addition of 3-cyanoindole to aromatic enones. *Synlett* **2017**, *28*, 1227−1231.
(59) Chaudhuri, M. K.; Hussain, S.; Kantam, M. L.; Neelima, B. Boric acid: a novel and safe catalyst for aza-Michael reactions in water. *Tetrahedron Lett.* **2005**, *46*, 8329−8331.
(60) Payra, S.; Saha, A.; Banerjee, S. On-water magnetic $NiFe_2O_4$ nanoparticle-catalyzed Michael additions of active methylene compounds, aromatic/aliphatic amines, alcohols and thiols to conjugated alkenes. *RSC Adv.* **2016**, *6*, 95951−95956.
(61) Ai, X.; Wang, X.; Liu, J.-m.; Ge, Z.-m.; Cheng, T.-m.; Li, R.-t. An effective aza-Michael addition of aromatic amines to electron-deficient alkenes in alkaline Al_2O_3. *Tetrahedron* **2010**, *66*, 5373−5377.
(62) Montini, T.; Melchionna, M.; Monai, M.; Fornasiero, P. Fundamentals and catalytic applications of CeO_2-based materials. *Chem. Rev.* **2016**, *116*, 5987−6041.
(63) Jayakumar, G.; Albert Irudayaraj, A.; Dhayal Raj, A. A comprehensive investigation on the properties of nanostructured cerium oxide. *Opt. Quantum Electron.* **2019**, *51*, 312.

https://doi.org/10.1021/acsomega.2c04614
ACS Omega 2022, 7, 42126−42137

(64) Tsunekawa, S.; Fukuda, T.; Kasuya, A. Blue shift in ultraviolet absorption spectra of monodisperse CeO_{2-x} nanoparticles. *J. Appl. Phys.* **2000**, *87*, 1318−1321.
(65) Tamizhdurai, P.; Sakthinathan, S.; Chen, S.-M.; Shanthi, K.; Sivasanker, S.; Sangeetha, P. Environmentally friendly synthesis of CeO_2 nanoparticles for the catalytic oxidation of benzyl alcohol to benzaldehyde and selective detection of nitrite. *Sci. Rep.* **2017**, *7*, 46372.
(66) Bhargava, R.; Shah, J.; Khan, S.; Kotnala, R. K. Hydroelectric cell based on a cerium oxide-decorated reduced graphene oxide (CeO_2−rG) nanocomposite generates green electricity by room-temperature water splitting. *Energy Fuels* **2020**, *34*, 13067−13078.
(67) Thommes, M.; Kaneko, K.; Neimark, A. V.; Olivier, J. P.; Rodriguez-Reinoso, F.; Rouquerol, J.; Sing, K. S. W. Physisorption of gases, with special reference to the evaluation of surface area and pore size distribution (IUPAC Technical Report). *Pure Appl. Chem.* **2015**, *87*, 1051−1069.
(68) Zhang, D.; Fu, H.; Shi, L.; Pan, C.; Li, Q.; Chu, Y.; Yu, W. Synthesis of CeO_2 nanorods via ultrasonication assisted by polyethylene glycol. *Inorg. Chem.* **2007**, *46*, 2446−2451.
(69) Maslakov, K. I.; Teterin, Y. A.; Popel, A. J.; Teterin, A. Y.; Ivanov, K. E.; Kalmykov, S. N.; Petrov, V. G.; Petrov, P. K.; Farnan, I. XPS study of ion irradiated and unirradiated CeO_2 bulk and thin film samples. *Appl. Surf. Sci.* **2018**, *448*, 154−162.
(70) Aggett, K.; Davies, T. E.; Morgan, D. J.; Hewes, D.; Taylor, S. H. The Influence of precursor on the preparation of CeO_2 catalysts for the total oxidation of the volatile organic compound propane. *Catalysts* **2021**, *11*, 1461.
(71) Umar, A.; Almas, T.; Ibrahim, A. A.; Kumar, R.; AlAssiri, M. S.; Baskoutas, S.; Akhtar, M. S. An efficient chemical sensor based on CeO_2 nanoparticles for the detection of acetylacetone chemical. *J. Electroanal. Chem.* **2020**, *864*, 114089.
(72) Liang, X.; Quan, N.; Wang, J.; Yang, J. Highly efficient heterogeneous procedure for the conjugate addition of amines to electron deficient alkenes. *Sci. China Ser. B-Chem.* **2009**, *52*, 874−878.

https://doi.org/10.1021/acsomega.2c04614
ACS Omega 2022, 7, 42126−42137